

ChemComm

Accepted Manuscript



This is an *Accepted Manuscript*, which has been through the Royal Society of Chemistry peer review process and has been accepted for publication.

Accepted Manuscripts are published online shortly after acceptance, before technical editing, formatting and proof reading. Using this free service, authors can make their results available to the community, in citable form, before we publish the edited article. We will replace this *Accepted Manuscript* with the edited and formatted *Advance Article* as soon as it is available.

You can find more information about *Accepted Manuscripts* in the [Information for Authors](#).

Please note that technical editing may introduce minor changes to the text and/or graphics, which may alter content. The journal's standard [Terms & Conditions](#) and the [Ethical guidelines](#) still apply. In no event shall the Royal Society of Chemistry be held responsible for any errors or omissions in this *Accepted Manuscript* or any consequences arising from the use of any information it contains.

COMMUNICATION

Synchronized Synthesis of Pd@C-RGO Carbocatalyst for Improved Anode and Cathode Performance for Direct Ethylene Glycol Fuel Cell

Cite this: DOI: 10.1039/x0xx00000x

Ramanujam Kannan,^a Kim Ae Rhan,^b Kee Suk Nahm^{a,c}, Hong-Ki Lee^d and Dong Jin Yoo^{a,c*}Received 00th January 2012,
Accepted 00th January 2012

DOI: 10.1039/x0xx00000x

www.rsc.org/

The simultaneous formation of the 5-nm sized Pd nanoparticles assembled in the flower shaped @carbon-reduced graphene oxide (Pd@C-RGO) carbocatalyst is synthesized via the solid state process between 1 and 2 minutes followed by microwave irradiation and exhibits improved electrocatalytic performance for the oxidation of ethylene glycol.

Low temperature direct alcohol fuel cells (DAFCs) have been increasingly catching the attention of researchers over the recent decades due to their high power density, low/zero emission pollutants, operation at low temperature (50-200 °C), easy storage and fuel handling. New technological developments have also led to the use of the DAFCs as a power source for portable applications [1-5].

Platinum nanoparticles (Pt NPs) are well accepted as the best catalysts for fuel cells. Although they suffer from CO deactivation and are susceptible to the time-dependent drift. Besides, the high cost and limited availability of Pt in nature remain the major obstacles to mass marketing the fuel cells, great efforts have been taken to produce an economical and efficient nanocatalyst [1, 2, 4]. As the Palladium NPs (Pd NPs) boast greater abundance and exert a high electrocatalytic effect on small organic molecules. They appear to be a potential substitute for Pt. However, it becomes necessary to further maximize the Pd activity and minimize its use, in order to help to reduce the cost of the fuel cells [1, 2, 5]. Thus, the supported nanocatalyst was constructed.

^a R&D Education Center for Specialized Graduate School of Hydrogen and Fuel Cells Engineering, ^b Graduate School, Department of Energy Storage/Conversion Engineering, Hydrogen and Fuel Cell Research Center, ^c Department of Chemistry, Chonbuk National University, Jeollabuk-do, 561-756, Korea
Email: djyoo@jbnu.ac.kr

^dHydrogen Fuel Cell Parts and Applied Technology Regional Innovation Center, Woosuk University, Jeollabuk-do 565-902, Korea.

† Electronic Supplementary Information (ESI) available: [See DOI: 10.1039/c000000x/]

Developing a an easy, new and low cost method of loading the highly active nanostructured Pd onto the supporting nanomaterials, with a high surface area and electrical conductivity is the most pressing need today [1-5]. Carbon materials such as conductive carbon, carbon nanotubes, carbon nanofibers, graphene (GR) etc., are the commonly used support materials [6]. Recently, GR has attracted tremendous attention as a support material for the metal NPs for energy storage and conversions. GR has opened up a new avenue for the use of 2D carbon materials as catalyst supports due to their intrinsic properties of good electrical conductivity, superior thermal and chemical stability, high surface area, and low fabrication cost [7, 8]. One of the most popular methods for the synthesis of the metal nanoparticle supported GR nanocomposite is the process of chemical reduction using metal salts with the GO in an aqueous medium. In this medium, the metal NPs aggregate to form larger metallic clusters [9] with broader distribution in size and shape on the GR surface, resulting in a decrease in the catalytic activity. To overcome this problem, the controlled synthesis of metal NPs assumes great importance to achieve maximum efficiency. A chemical reduction method using common reducing agents such as hydrazine and sodium borohydride is employed for the reduction of both the metal and the GO [10, 11]. However, these reducing agents are hazardous and/or toxic. Therefore, an inexpensive and large scale production of an eco-friendly reduced GO (RGO)-metal nanocatalyst for commercial usage becomes imperative in the present scenario [12, 13]. Recently, RGO and/or metal NPs have been synthesized using various green reducing agents such as sugar, wild carrot, ascorbic acid (AA) and amino acids etc., [14-19]. Of these, AA shows excellent reduction activity on both the metal and graphene oxide. Earlier studies on the reduction reaction performed in an aqueous medium [14,15] revealed that the AA has a strong affinity with the aqueous medium [12], resulting in the formation of metallic clusters, albeit with reduced catalytic activity. Besides this, different by-products are formed during the reaction process which could disturb the reaction and/or lower the catalytic activity of the catalyst. Therefore, we attempted to utilize these by-products converting them into carbonaceous material. The advantage of an *in situ* generation of carbonaceous material offers a strong affinity with the metal NPs and the support [6, 20-26]. In line with this fact, the microwave assisted *in situ* generation of the carbonaceous materials was derived from the AA on carbon supports such as GO, multiwalled carbon

nanotubes (MWCNT) and Vulcan XC (VXC) carbon. The Pd NPs were generated on the support materials by a simple, green and cost effective method within a very short time. The detailed synthesis and characteristics are presented in the support information (ESI[†]). The Pd@C-RGO carbocatalyst prepared was tested for its potential use as an electrocatalyst for the ethylene glycol (EG) oxidation, resulting in the prepared catalyst exhibiting enhanced catalytic activity. The catalyst formation and enhanced catalytic activity were explained by a suitable mechanism.

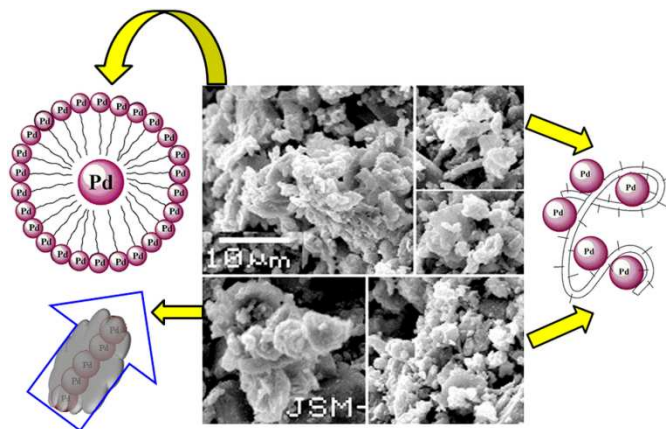


Fig. 1 SEM images of Pd NPs formation using AA by solid state process.

The prepared GO (GS1), Pd NPs grafted GO by the solid state reaction (GS2) and the solution state reaction (GS3) methods with AA were analyzed by powder X-ray diffraction. A strong and sharp peak at 11.3° (002) was detected in the XRD pattern of GO (GS1), which corresponds to the AB stack structure of the GO with the intercalated water and oxygen functionalities (Fig. S1, ESI[†]). The disappearance of the peak at 11.3° and the emergence of the new broad peak at $\sim 25^\circ$, observed for samples GS2 (Fig. S1(b)) and GS4 (Fig. S1(d)) indicate the reduction of the GO to RGO. The decrement in the GO intensity indicates the removal of water and oxygen functionalities with exfoliation RGO layers of during the reduction process. The broad peak at $\sim 25^\circ$ indicates that the graphene flakes are randomly oriented in the stacking direction in the RGO [12]. The Pd NPs over the RGO prepared by the solid state process revealed the characteristic diffraction peaks at 40.1° , 45.6° and 68.2° , pertaining to the (111), (200) and (220) planes, respectively, of the cubic Pd NPs, while the broad peak at $\sim 25^\circ$ indicates the RGO formation (Fig. S1 GS2 ESI[†]). At the same time, in the solution process (Fig. S1, GS3), the characteristic XRD patterns observed for the GO, RGO and Pd NPs at (2θ) 11.3° , $\sim 25^\circ$ and 42.1° respectively, indicates the occurrence of a partial reduction of the GO and Pd. The solid state reduction method enabled the complete reduction of the GO to RGO in the absence of the metal salt (GS4). Based on the XRD results, the GS1, GS2, GS3 and GS4 samples are labeled GO and Pd@C-RGO, Pd-PRGO (partially reduced GO/Pd) and RGO, respectively. The catalyst (Pd@C-RGO) prepared by the microwave irradiation process shows the XRD peaks at (2θ) 19.8° (110), 20.1° (111), 27.8° (104), 30.1° (210), 35° (301) for carbon with a marginal shift in the peak positions, in addition to that of the XRD peak position of the Pd NPs observed at 39.4° instead of at 40.1° , indicates the formation of the Pd@C [27] (Fig. S2, ESI[†]). The prepared Pd@C-RGO carbocatalyst was further analyzed by absorption spectroscopic methods (ultra violet-visible spectroscopy Fig. S3 and Fourier transform infrared spectroscopy Fig. S4, ESI[†]).

Recent studies explained the formation of the metal NPs [Pt, silver (Ag) and gold (Au)] using AA in an aqueous medium [16, 25]. However, the AA and metal has a strong affinity with the water molecules [12] resulting in a slow reduction process. However, in the solid state reaction the formation of the AA complex with the Pd²⁺ complex is fast, producing of size-controlled Pd NPs, the GO also was reduced to RGO. The Pd@C is synthesized by polymerization followed by the carbonization process. The color change from gray to black and the jelly-like character of the mixture, within a brief 1-2 minutes period, indicates that the reaction is fast at room temperature. The color change and transformation to the jelly-like texture indicates the simultaneous reduction of the Pd and GO by the oxidation of AA and its subsequent polymerization. The Pd NPs formation is analyzed using SEM. As evident from the Fig. 1, the Pd NPs are formed by three different orientations, self-assembly of the metal NPs in the flower-like architectural form, the Pd NPs encapsulation by the polymerized by-product of AA i.e., dehydroascorbic (DHA) acid and/or AA. However, the precise mechanism of the formation remains unclear and we presumed that, during the solid state process the AA oxidizes into DHA [16] and this DHA covers the Pd NPs to control the aggregation.

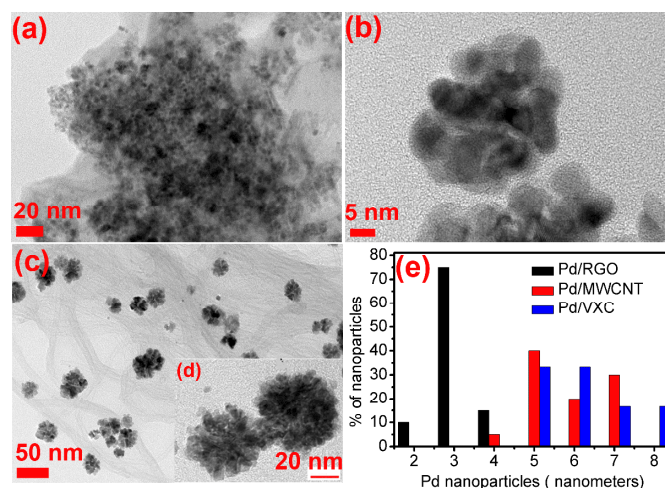


Fig. 2 TEM micrographs of (a) Pd/RGO, (b) Pd@C-RGO, (c and d) Pd@C-MWCNT and (e) Pd NPs distribution over the supports.

TEM studies reveal the formation of spherical-shaped Pd NPs uniformly distributed over the RGO (Fig. 2a). Further, on heating with microwave irradiation, the DHA gets converted into the carbon material exhibiting a flower-like morphology (Fig. 2b). This is attributed to the DHA present along with the Pd NPs, which gets carbonized during the microwave process, this carbon assembles the Pd particles to the flower-like architecture (Fig. 2b). The carbon formation was clearly observed in the TEM image (Fig. S5, ESI[†]). Also, on the MWCNT and VXC (Figs. 2 c&d) the Pd NPs were assembled as uniform flower-like architecture ranging from 20-40 nm in size, besides the individual particle retains its size (3-10 nm) and shape. The EDS spectra of indicates that the C content of Pd/RGO and Pd@C-RGO are 46.67% and 51.99%, respectively (Fig. S6, ESI[†]). The Raman spectra for the GO exhibits two characteristic Raman peaks of the D (1359 cm^{-1}) and G (1593 cm^{-1}) bands [12]. The intensity of D and G bands (I_D/I_G) ratio for GO, RGO, Pd-RGO and Pd@C-RGO are 0.9901, 1.0784, 1.0780 and 0.9159, respectively. The I_D/I_G ratios of the RGO, Pd-RGO are increased compared with the GO, which indicates the formation of structural defects in the GO sheets during the reduction process, whereas the I_D/I_G ratio of the Pd@C-RGO is very minimum at 0.9159 compared

with that of the GO, RGO and Pd-RGO. This is attributed to the carbon formed during the microwave irradiation (Fig. S7, ESI[†]).

The C1s deconvoluted XPS spectra of the GO, Pd-RGO and Pd@C-RGO samples (Fig. S8 and Fig. S9, ESI[†]), in which the peak at ca. 284.3 eV attributed to the binding energy of C1s is further separated into three peaks at 284.3, 286.3 and 288.3 eV, corresponding to the C-C/C=C, C-O and O-C=O, respectively. In GO, the oxygen-containing functional groups are predominantly present; hence, the 286.3 eV intensity is higher. This was further confirmed by thermogravimetric analysis (Fig. S10 and Fig. S11, ESI[†]). However, in the Pd-RGO and Pd@C-RGO samples, the peak intensity at 286.3 eV is reduced, indicating the absence of the hydroxyl functional groups in the material. This indicates that an effective reduction reaction process had occurred. After the microwave irradiation, apart from the C/C=C (284.3 eV), C-O (286.1 eV) and O-C=O (287.1 eV) peaks, a new peak is observed at ca. 282.2 eV, indicating the presence of the carbon product over the Pd in the sample [27]. The carbon formation (i.e., Pd@C) is further confirmed by the peak observed at 533.1 eV of the deconvoluted O 1s spectra (Fig. S8) [28]. In all the three samples, the Pd 3d spectra shows similar XPS spectra. The peaks located at 335.1 eV and 341.1 eV are the binding energies of the Pd 3d_{5/2} and Pd 3d_{3/2}, respectively, demonstrating the presence of the Pd NPs over the catalyst (Fig. S9, ESI[†]).

The carbocatalysts thus prepared were subjected to the electrocatalytic oxidation of the EG, oxygen evolution reaction (OER) and oxygen reduction reaction (ORR). The Pd@C-RGO and Pd@C-MWCNT electrodes exhibits higher oxygen evolution and oxygen reduction current when compared with the Pd@C-VXC electrode [Fig. 3a (i, ii and iii)]. The EG oxidation was performed in the (Fig. 3b) Pd@C-VXC, (Fig. 3c) Pd@C-MWCNT and (Fig. 3d) Pd@C-RGO carbocatalyst electrodes in the 0.5 M EG + 1 M KOH solution. All these three catalysts showed similar electrocatalytic activity with different peak current responses to the EG oxidation. The Pd@C-RGO carbocatalyst shows a higher peak current response than the Pd-RGO (Fig. S12). The onset potential for the EG oxidation began at -0.5 V in the Pd@C-MWCNT and Pd@C-RGO, which was much earlier than the Pd@C-VXC (-0.28 V) (Fig. S13a, ESI[†]). In general, the intermediates formed during the forward scan get oxidized in the reverse scan. However, in the present study, most of the intermediates were oxidized in the forward scan itself. The ratio between the forward (I^f) and backward peak current (I^b) response, i.e., I^f/I^b of 6.6, 7.5 and 8.7 for Pd@C-VXC, Pd@C-MWCNT and Pd@C-RGO, respectively, indicates a higher tolerance of the Pd@C-RGO to the poisoning intermediates than the VXC and MWCNT supported Pd@C. The Pd@C-RGO exhibits a higher OER current and most of the intermediates are oxidized during the forward scan, thus resulting in a higher tolerance.

We extended the CV potential range, and the large anodic current which appeared when the electrode potential was scanned between -1.1 V and +1.0 V, indicated the occurrence of the OER on the electrode surface (S13b, ESI[†]). Furthermore, the oxygen evolved could be reduced, leading to a cathodic current peak in the oxygen reduction regime with a higher peak current response. It was found that the electrocatalytic activity of both the OER and ORR was higher in the Pd@C-RGO than in the Pd@C-MWCNT, Pd@C-VXC carbocatalyst and the glassy carbon electrode (Fig. S13b, ESI[†]). This higher catalytic activity and tolerance towards electrode poisoning are due to the *in situ* generated carbon, which facilitates the electron transfer between the catalyst and the electrode. These results suggest that the electrocatalysts prepared are highly active and can be used

as both anode and cathode materials for the DAFCs. The prepared Pd@C-RGO exhibits a higher catalytic response to the reduction of 4-nitrophenol in a short time period (5 s) (Fig. S14, ESI[†]). Similarly, we attempted to synthesize Pt, Au, and Ag NPs over the carbon supports. Of these, the Ag NPs were observed to be formed over the GO within a very short time ca. of 1 to 2 minutes Whereas, the Au and Pt formation took at least 3-5 minutes of time. On the other hand, at elevated temperatures (> 80 °C), the formation of Au and Pt NPs over the carbon was much faster. Detailed investigations are currently under progress.

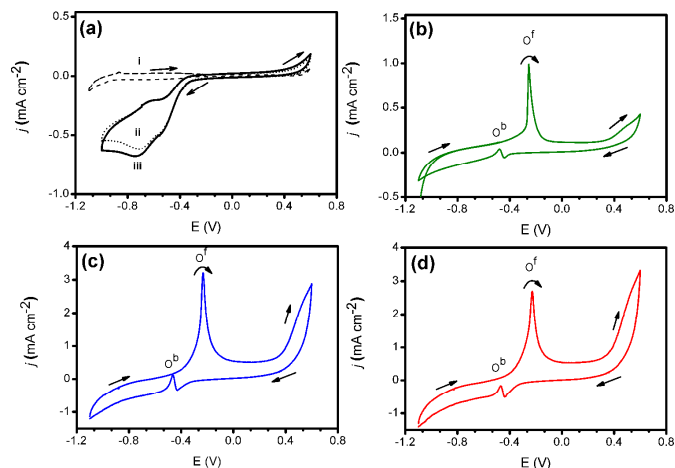


Fig. 3 (a) CVs for the electrochemical behavior of (i) Pd@C-VXC, (ii) Pd@C-MWCNT, and (iii) Pd@C-RGO carbocatalyst in N₂ saturated 1 M KOH. Electrooxidation of EG at (b) Pd@C-VXC, (c) Pd@C-MWCNT, and (d) Pd@C-RGO carbocatalyst in nitrogen saturated 0.5 M EG + 1 M KOH solution.

In brief, we demonstrated the synchronized synthesis of the Pd@C over the RGO, MWCNT and VXC carbon using AA as a green reducing agent, by the solid state process, at room temperature (25±2 °C). The solid-state reduction process yielded Pd-RGO, where both the metal and GO were reduced to Pd-RGO. The enhanced electrocatalytic activity of the Pd@C-RGO could be attributed to the smaller particle size of the Pd NPs (5 nm) and the improved surface area provided by the support (RGO). In addition, an excellent catalytic activity towards the reduction of 4-nitrophenol was observed. The present work is expected to provide a simple and interesting way of generating metallic NPs supported graphene on a large-scale and which could offer extensive application in energy and environmental applications.

The work was supported by the Human Resources Development Program (No. 20134030200330) of the Korea Institute of Energy Technology Evaluation and Planning (KETEP) grant funded by the Korea Government Ministry of Trade, Industry and Energy. The work was supported by the Program of RIC (Woosuk University), conducted by the Ministry of Knowledge Economy of the Korean Government.

Notes and references

1. S. Sharma, and B. G. Pollet, *J Power Sources*, 2014, **208**, 96.
2. R. Kannan, A.E. Kim, and D. J. Yoo, *J. Appl. Electrochem.*, 2014, **2**, 267.
3. G. Z. Hu, F. Nitze, X. Jia, T. Sharifi, H. R. Barzegar, E. G. Espino, and T. Wagberg, *RSC Adv.*, 2014, **4**, 676.

4. R. Reichert, J. Schnaidt, Z. Jusys, and R. J. Behm, *Phys. Chem. Chem. Phys.*, 2014, **16**, 13780.
5. C. Bianchini, and P. K. Shen, *Chem. Rev.*, 2009, **109**, 4183.
6. J. M. Campelo, D. Luna, R. Luque, J. M. Marinas, and A. A. Romero, *Chemosuschem*, 2009, **2**, 18.
7. D. Chen, H. Feng, and J. Li, *Chem. Rev.*, 2012, **112**, 6027.
8. K. Thiagarajan, A. Ananth, B. Saravanakumar, Y. S. Mok, and S. J. Kim, *Carbon*, 2014, **78**, 25.
9. A. Ramasubbu, A. Vanangamudi, S. Muthusubramanian, M. S. Ramachandran, and S. Sivasubramanian, *Electrochem. Commun.*, 2000, **2**, 56.
10. H. J. Shin, K. K. Kim, A. Banayad, S. M. Yoon, H. K. Park, I. S. Jung, M. H. Jin, H. K. Jeong, J. M. Kim, J. Y. Choi, and Y. H. Lee, *Adv. Funct. Mater.*, 2009, **19**, 1987.
11. S. Stankovich, D. A. Dikin, R. D. Piner, K. A. Kohlhaas, A. Kleinhammes, Y. Jia, Y. Wu, S. T. Nguyen, and R. S. Ruoff, *Carbon*, 2007, **45**, 1558.
12. S. Bose, T. Kuila, A. K. Mishra, N. H. Kim, and J. H. Lee, *J. Mater. Chem.*, 2012, **22**, 9696.
13. S. Yang, J. Dong, Z. Yoo, C. Shen, X. Shi, Y. Tian, S. Lin, and X. Zhang, *Sci. Rep.*, 2014, **4**, doi: 10.1038/srep04501.
14. C. Zhu, S. Guo, Y. Fang, and S. Dong, *ACS nano*, 2010, **4**, 2429.
15. Y. Zhou, D. Wang, and Y. Li, *Chem. Commun.*, 2014, **50**, 6141.
16. S. H. Kim, G. H. Jeong, D. Choi, S. Yoon, H. B. Jeon, S. M. Lee, and S. W. Kim, *J. Colloid. Inter. Sci.*, 2013, **89**, 85.
17. G. H. Jeong, D. Choi, M. Kang, J. Shin, J. G. Kang, and S. W. Kim, *RSC Adv.*, 2013, **3**, 8864.
18. A. Zhang, M. Liu, M. Liu, Y. Xiao, Z. Li, J. Chen, Y. Sun, J. Zhao, S. Fang, D. Jia, and F. Li, *J. Mater. Chem. A*, 2014, **2**, 1369.
19. A. Kumar, and M. Khandelwal, *New. J. Chem.*, 2014, **38**, 3457.
20. R. Kou, Y. Shao, D. Mei, Z. Nie, D. Wang, C. Wang, V. V. Viswanathan, S. Park, I. A. Aksay, Y. Lin, Y. Wang, and J. Liu, *J. Am. Chem. Soc.*, 2011, **133**, 2541.
21. Y. J. Zhu, and F. Chen, *Chem. Rev.*, 2014, **114**, 6462.
22. Y. Lin, D. W. Baggett, J. W. Kim, E. J. Siochi, and J. W. Connell, *ACS Appl. Mater. Inter.*, 2011, **3**, 1652.
23. D. J. Xue, S. Xin, Y. Yan, K. C. Jiang, Y. X. Yin, Y. G. Guo, and L. J. Wan, *J. Am. Chem. Soc.*, 2012, **134**, 2512.
24. B. Li, H. Cao, J. Shao, and M. Qu, *Chem. Commun.* 2011, **47**, 10374.
25. A. Murugadoss, R. Pasricha, and A. Chattopadhyay, *J. Colloid. Sci. Inter.*, 2007, **311**, 303.
26. T. Sun, Z. Zhang, J. Xiao, C. Chen, F. Xiao, S. Wang, and Y. Liu, *Sci. Rep.*, 2013, **3**, 2527.
27. Y.-F. Han, D. Kumar, C. Sivadinarayana, A. Clearfield, and D. W. Goodman, *Catal. Lett.*, 2004, **94**, 131.
28. G. Beamson, and D. Briggs, *High resolution XPS of organic polymers- the scienta ESCA 300 database*, Wiley Interscience, 1992, appendices 3.1 and 3.2.